PROCEEDINGS, Eleventh Workshop on Geothermal Reservoir Engineering
Stanford University, Stanford, California, January 21-23, 1986
SGP-TR-93

DUAL PERMEABILITY MODELING OF FLOW IN A FRACTURED GEOTHERMAL RESERVOIR

John D. Miller and David W. Allman

Idaho National Engineering Laboratory
Idaho Falls, ID 83415

ABSTRACT

A three dimensional fracture system synthesis and flow simulation has been developed to correlate drawdown characteristics measured in a geothermal well and to provide the basis for an analysis of tracer tests. A new dual permeability approach was developed which incorporates simulations at two levels to better represent a discrete fracture system within computer limitations. The first incorporates a discrete simulation of the largest fractures in the system plus distributed or representative element simulation of the smaller fractures. The second determines the representative element properties by discrete simulation of the smaller fractures. The fracture system was synthesized from acoustic televiewer data on the orientation and separation of three distinct fracture sets, together with additional data from the literature. Lognormal and exponential distributions of fracture spacing and radius were studied with the exponential distribution providing more reasonable results. Hydraulic apertures were estimated as a function of distance from the model boundary to a constant head boundary. Mean values of 6.7, 101 and 46 μm were chosen as the most representative values for the three fracture sets. Recommendations are given for the additional fracture characterization needed to reduce the uncertainties in the model.

INTRODUCTION

The objective of the work presented in this paper is to model the flow system in the vicinity of a geothermal well as the basis for a subsequent correlation of measured tracer responses. Data from Raft River Well RRGP-5B was used as the basis for the study. This well was tested in September through November, 1982 as part of a Department of Energy research program on the injection of spent geothermal fluids. A series of drawdown tests were conducted along with a number of injection-backflow tracer tests. This analysis is part of an ongoing effort, incorporating field studies and analytic, physical model and computer simulation, which is directed towards an understanding of the processes controlling the movement of fluids in a geothermal reservoir. The following sections provide a summary of the modeling approach and its computer implementation, the RRGP-5B borehole characterization, fracture system synthesis and flow correlation, and recommendations for further fracture characterization.

MODELING APPROACH

The fluid transport system in a fractured geothermal reservoir is composed of interconnected conduits ranging in scale from major fault zones through large fractures down to microcracks with a minimum aperture for flow of 0.2 μm (Romm, 1966). The challenge presented to the flow modeler is the necessity of explicitly simulating the upper portion of this range within computer memory and run cost limitations. Solute and heat transport present an even larger challenge since the majority of the rock surface for heat transfer and sorption occurs in the smaller end of this flow range. In addition the microcracks smaller than 0.2 μm must be included as the host for the "matrix" diffusion process.

The approach in this work is an extension of earlier work on two-dimensional models by Miller (1983), Clemo (1985), and Hull (1985). The analytic basis for the approach is given by Clemo (1986). Fractures are addressed in three different ranges of size, termed faults, global fractures, and distributed fractures. Faults are classified as those conduits sufficiently large as to provide a trivial head gradient for substantial flows. These elements are represented as constant head boundaries. They may either be deterministically identified from drilling, flow testing or geophysical methods or may be the largest elements of a complete probability distribution, if one could be defined. The global fractures are the next smaller set and are discretely described with properties chosen from probability distributions since they cannot, at this scale, be distributed and they cannot be specifically described. The distributed fractures are the remainder. They are incorporated in a representative element bounded by the global fractures. The properties of this representative element are found from a sub-scale model in which the smaller fractures are described

discretely. To summarize, the complete flow simulation incorporates two models: a large scale model which incorporates the well and the faults as its flow or head boundaries, the large fractures as discrete elements and the smaller fractures as representative or distributed elements. The second model describes the representative element with global fractures omitted and with the next smaller set of fractures modeled discretely. Each of these models is as detailed as possible within computer memory and cost limitations.

The model, of necessity, incorporates a number of approximations. As is common in the discrete fracture analysis and simulation literature, fractures are idealized as circular, parallel sided, planar discs. Real fractures are rough, curved or laterally stepped and are probably not circular due to interference with other fractures. Indeed, some fractures terminate on other fractures (Dershowitz et al., 1985). The model, in addition, neglects the variation of fracture orientation from the mean of each orientation set. The remainder of the geometric approximations have to do with the probability density distributions of spacing, radius and aperture which are discussed in a subsequent section.

Based on the subsequently described acoustic televiewer survey, the RRGP-5B fracture system model consists of a hydrofracture and three differently oriented probabilistic sets of parallel fractures. Each fracture is represented as a circular disc. Figure 1 shows the approach given by Huang and Evans (1985) and adopted for this study: a given fracture intersects another fracture (or the boundary of the model) in a line. The head is assumed constant over the length of the line and is located, for reference, at a node at its midpoint. A flow path exists in a fracture between two lines of intersection. Laminar flow is computed in this path using the cubic law (Lamb, 1945) in which flow varies as the cube of the aperture. The length of the path is the distance between nodes and the width is approximated as the average of the two intersection lengths, without consideration of their orientation. As shown in Figure 1, in a fracture with more than two intersections or nodes, a flow is computed independently between each node and every other node. Consideration of a more sophisticated model is deferred to future studies.

This analysis departs from the Huang and Evans approach in the inclusion of the distributed fracture flow paths. As described previously, the conductivities of these paths are determined from representative element simulations with fractures of global size excluded. Separate representative element simulations are conducted to determine

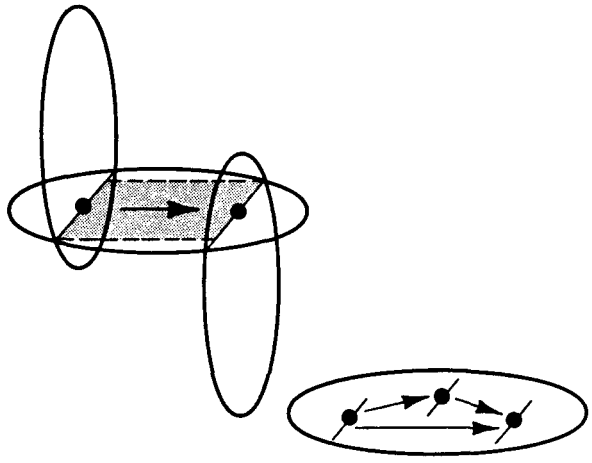

6 0290

Figure 1. Discrete Fracture Flow Paths

the conductivity normal to each of the three fracture sets. A hydraulic gradient is imposed normal to the set being evaluated. The thickness of the representative element model is an important parameter. As shown by Clemo (1986), the conductivity between two planes decreases with increasing separation between those planes because of the reduction in number of cross fractures large enough to directly span them. Thicknesses were chosen equal to the mean separation of the corresponding fracture set in the global model.

Figure 2 shows the computational process. Consider a fracture somewhat smaller than those included in the global model, which bridges two global fractures of a common

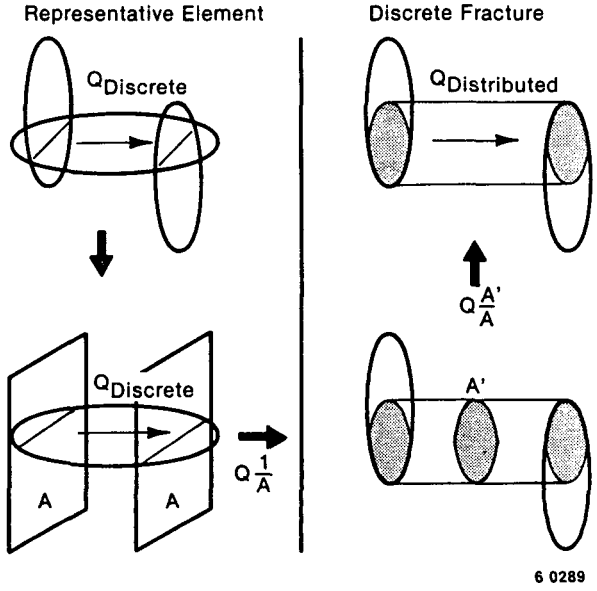

6 0289

Figure 2. Distributed Fracture Flow Paths

set. The contribution of this fracture to the conductivity between the two global fractures is computed discretely and is averaged, in the representative element, over the cross-sectional area of that model. Applying the resultant conductivity over the shadow or overlap area between the two global fractures in the discrete simulation then introduces the requirement that the distributed fracture lie in a region which intercepts both global fractures. The discrete pathway due to the small fracture has been replaced by the conditions that a fracture be long enough to bridge the gap and that it occurs in a suitable lateral position.

The determination of the distributed fracture paths to the hydrofracture is more complex since it is not parallel to any of the fracture sets. A probabilistic fracture is assigned a distributed fracture path to the hydrofracture if it shadows it without shadowing a fracture nearer to the hydrofracture. These calculations are made assuming all fractures parallel the hydrofracture. The path crossection is the area of the entire fracture as projected onto the plane of the hydrofracture and its length and conductivity are computed as before.

In all cases, distributed fracture flow is computed between the average heads for each of the two fractures. It should be noted that this calculation identifies the entire fracture as a pressurized body which receives or provides flow to the number of smaller fractures which intercept it.

COMPUTER IMPLEMENTATION

The conceptual model described above is implemented in a sequence of two codes which are together called FRACSL3D (FRactured media flow and transport - Advanced Continuous Simulation Language, 3D). The first code is initiated with a synthesis of fracture location, orientation and radius. Fracture centers are located, in directions parallel to the fracture plane, randomly throughout the model. As discussed subsequently, two different approaches were used to locate the fracture centers in the third (normal) direction.

After describing the hydrofracture and synthesizing the three probabilistic sets, the distributed fracture paths were found as described in the preceding section. The fracture-to-fracture and fracture-to-boundary intersections were then found using subroutines developed by Huang and Evans (1984). The fracture, distributed fracture path, and intersection information was then output to a data file.

The second code reads the data file and additional data, calculates the fracture paths and solves for the head and flow distributions. This program was developed at the Idaho National Engineering Laboratory as a series of subroutines with supporting routines from the ACSL (Advanced Continuous Simulation Language) problem solver code (Mitchell and Gauthier, 1981).

Apertures, widths, lengths, and conductivities are computed for the various fracture paths. Apertures are assumed to vary linearly with fracture radius with proportionality constants chosen as discussed subsequently. Fixed head or flux boundary conditions may be applied at any node. Alternatively, connection to a remote constant head boundary may be made by specifying the distance to that boundary. The path conductivity is assumed to be equal to the mean for the global fractures within the model.

A first order differential equation is written for the conservation of mass at each node and the steady state flow and head distribution is found by iterating to drive the head derivatives to zero. Both codes are implemented on a CDC CYBER 176 computer with 130,368 decimal words of small core available to the user. The flow code is limited to several hundred nodes while the synthesis code can analyze much larger systems. The total cost of the 13 computer runs providing the reported data was approximately $75. These costs are low enough to permit the multiple realizations necessary for some studies.

RRGP-5B BOREHOLE CHARACTERIZATION

Raft River Well RRGP-5B was completed in metasedimentary quartzite and schist at a depth of 4911 ft. An acoustic televiewer survey was made by the United States Geological Survey for a 495 foot borehole interval prior to well completion. A second survey of the production interval, made after the liner was installed and the well was hydrofractured, showed no new fractures other than the hydrofracture itself. A total of 142 discontinuities were found in the 495 foot pre-completion interval. Figure 3 shows a plot of the cumulative frequency of occurrence vs. separation distance for the region between 4445 and 4695 ft. This region was selected because it is homogeneous in fracture distribution and includes the observed portion of the hydrofracture below the liner and the postulated portion above the bottom of the liner. The data, shown for three orientation sets, are fitted by lognormal distributions. Table 1 summarizes the characteristics of the three fracture sets.

FRACTURE SYSTEM SYNTHESIS

As shown schematically in Figure 4, the model is established by describing the hydrofracture, a model space, and the probabilistic fractures within that space. Based on acoustic televiewer observations

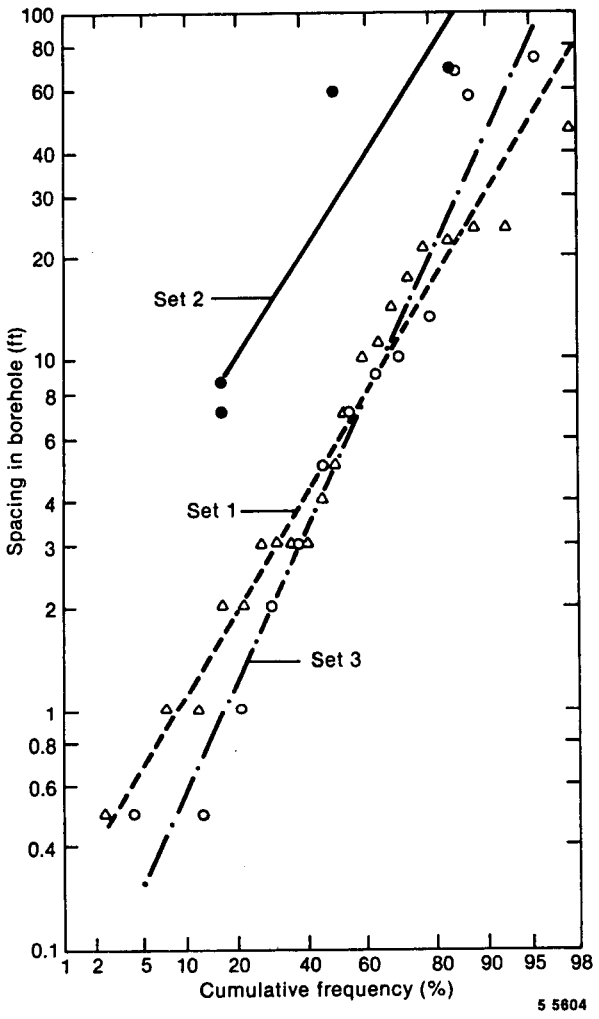

Figure 3. Fracture Spacing

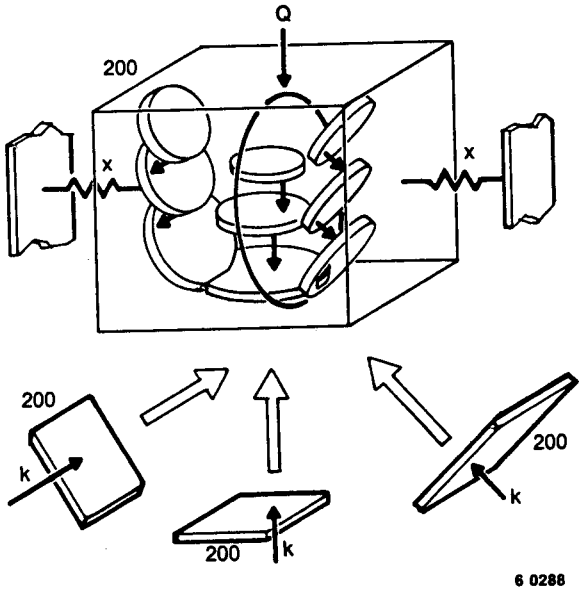

Figure 4. RRGP-5B Model

of the portion of the wellbore below the well liner, the hydrofracture was described as a 100 ft radius circle, centered on the bottom of the liner and oriented in a vertical plane with strike to the north. A cubic model space 200 ft on a side was chosen to surround the hydrofracture and thereby model the distribution of flow from the well through the hydrofracture and into the formation. This volume was centered on the bottom of the wellbore liner and oriented with vertical faces running N-S and E-W.

In the initial synthesis of probabilistic fractures, the spacing between successive members of the same set was based on the lognormal distribution shown in Figure 3 and Table 1. Since this distribution is that of a scanline (borehole) sampling, the spacing between fractures which are located laterally throughout the model region must be considerably smaller. The model separations were adjusted until scanline samplings equalled the measured mean separations.

These results are sensitive to the fracture radius distribution. Since radius distributions are not known for the Raft River fracture system, data on radius-to-spacing ratio from the literature was used. Mahtab et al. (1973) reported trace length, separation and physical apertures for a copper mine in a granite batholith. Three nearly orthogonal fracture sets were found in quartz monzonite and in monzonite porphyry. While the distributions were not fitted by the author, the means were given. The Mahtab et al. trace length means were first multiplied by .635 to provide the expected value of radius. The ratio of mean-radius-to-mean-spacing was found to be 3.16 when averaged over the 6 fracture set-rock type combinations. Gale et al. (1985) reported mean-radius-to-mean-separation values for the Stripa ventilation drift which average 1.15 for the four fracture sets. A value of 2.15 was assumed for the Raft River analysis as the mean of the values from the literature. The distribution, for the first analysis, was assumed to be lognormal.

Fractures were synthesized within a 300 ft. cube centered on and parallel to the model cube. The additional space was provided to extend fractures into the model from centers located outside it. Synthesis and scanline studies were conducted separately for each of the three fracture sets.

In order to reduce the number of nodes to the capability of the flow code, it was necessary to limit the fractures to those larger than 250 ft. radius. Two observations can be made from this result. The first is that the resulting model is unsatisfactory since the extra fracture generating space outside the model only provides for fractures

TABLE 1

WELL RRGP-5B FRACTURE SET CHARACTERISTICS
DEPTHS 4445-4695 ft

Set	Number of Separations	Strike	Dip	Borehole Spacing: Mean of $\log_{10}$ ft	Borehole Spacing: std dev of $\log_{10}$ ft	Mean Normal[1] Spacing ft
1	21	N12W	79E	.753	.539	2.036
2	3	N34E	46E	1.480	.551	30.77
3	12	N18W	20E	.701	.708	14.17

(1) normal spacing = (borehole spacing) (cos dip)

with radii less than 50 feet. The more significant observation is that the synthesized fracture system is dominated, probably excessively so, by large fractures. Reduction of the mean-radius-to-mean-spacing ratio of 2.15 would probably not affect the results significantly since a larger number of fractures would then be required to provide the required scanline spacing.

While the acoustic televiewer spacing data is obviously well fitted by the lognormal characteristic shown in Figure 3 it should be noted that the smaller fractures may not be detected. In the literature as reviewed by Evans (1983), scanline length distributions were best fitted by a lognormal distribution by some researchers while an exponential distribution provided the best fit to data for others. In addition, a power law distribution with probability varying with trace length to an exponent varying between -1.3 and -1.8 was found best by Segall and Pollard (1983). The analysis of fracture permeability at the Stripa ventilation draft by Gale et al. (1985) utilized both lognormal and exponential distributions.

As an alternative, a second analysis was performed for exponential distributions of spacing and radius, again differing by a factor of 2.15. The exponential spacing was provided by randomly locating the fracture centers in the normal direction (Priest and Hudson, 1981). The single parameter in the exponential distribution of the spacing, the mean value, was chosen as the arithmetic mean of the measured spacings. Fractures are located randomly in the three directions until a scanline has accumulated the number of interceptions which provide the required mean spacing. This procedure was modified analytically to avoid treating the very large number of small fractures which would not intercept the scanline. The distribution of radii was limited to the larger values and the mean spacing for the scanline was increased accordingly. After providing for the correct scanline sampling rate, the fractures simulated discretely in the global analysis were limited to those greater than 100 ft radius to provide a manageable global flow model. The three representative elements shown schematically in Figure 4 were then developed using the same distributions. Fracture radii were limited to 100 ft at the maximum and minimums of 27 to 32 ft. Table 2 summarizes the four geometric models. While these calculations would normally be made on the basis of the mean of a number of fracture system realizations, the fracture system statistics are not sufficiently well defined to warrant the refinement.

FLOW CORRELATION

Drawdown tests were conducted at well RRGP-5B at flow rates ranging from 75 to 300 gpm. Steady-state conditions were reached in an average of 235 seconds after the start of drawdown and the well recovered to the initial condition in an average of 130 seconds after the end of production. Figure 5 shows the variation with flow rate of drawdown and recovery heads at steady-state. The drawdown and recovery heads are essentially identical and the mean values rise with increasing flow at a rate greater than linear. The formation characteristics, found by subtracting a calculated wellbore loss, also rises at a greater than linear rate, showing the presence of non-linear or turbulent flow in the formation. A linear formation drawdown was estimated by drawing a tangent to the initial portion of the formation curve.

Predicted drawdowns were found by solving for the flow distributions in the four geometric models previously described. The individual representative element models were used to evalute the conductivity normal to the hydrofracture and fracture sets 2 and 3. Distributed flow between global

TABLE 2

GLOBAL AND REPRESENTATIVE ELEMENT MODELS
EXPONENTIAL DISTRIBUTION OF SPACING AND RADIUS

Model	Fracture[1] Generating Region - ft	Model[1][2] Region - ft	Fracture Radius-ft	# Fractures	# Internal Nodes	# Boundary Nodes	# Discrete Fracture Paths	# Distributed Fracture Paths	Representative Element[4] Conductivity ft/day
Global	600/600/600	200/200/200	above 100	31	64	102	765	14	---
Element[3] 1	400/250/400	200/50/200	32 to 100	33	32	114	294	--	.0472
Element 2	238/400/400	38/200/200	27 to 100	23	20	98	131	--	.0209
Element 3	239/400/400	39/200/200	27 to 100	26	41	98	310	--	.2520

(1) x by y by z

(2) model region centered in fracture generating region

(3) representative element for conductivity normal to hydrofracture

(4) through smallest model dimension; at aperture-to-radius ratio = .5E-5

fractures in set 1 was neglected since these fractures are widely separated. Flow solutions for the three representative element models yielded conductivities for a particular aperture-to-radius value. These conductivities were then incorporated in the global model where a single value of aperture-to-radius ratio was used to adjust the apertures and the conductivity of both representative element fractures and global fractures. The selection of a distance from the model boundary to a remote, fixed-head boundary completes the input set and a flow solution is obtained. Since all component head rises are dependent on the cube of the aperture, system head rises for other values of aperture-to-radius ratio are obtained by a simple ratio.

The contribution of the representative element to the computed drawdown was found by zeroing the representative element conductivities used in the global flow simulation. The drawdown head increased by 9.0%, corresponding to the cube of the ratio of the dominant apertures in the representative element models to those in the global model.

Flow calculations, for both global and representative element models, were based on linear flow between smooth parallel plates. However, the existence of non-linear flow in some of the fracture paths is shown by the non-linear drawdown characteristic given in Figure 5. As summarized by Gale et al. (1985), the onset of non-linear flow has been observed at a Reynolds number of 80 at a relative roughness of 1.0 and at about 100 at a relative roughness of 0.862. The average Reynolds number over the 534 discrete fracture paths in the global model is 10.5, based on a hydraulic diameter equal to twice the aperture. This value is independent of the aperture values for a system otherwise fixed in flow and geometry. True Reynolds numbers, however, range to considerably

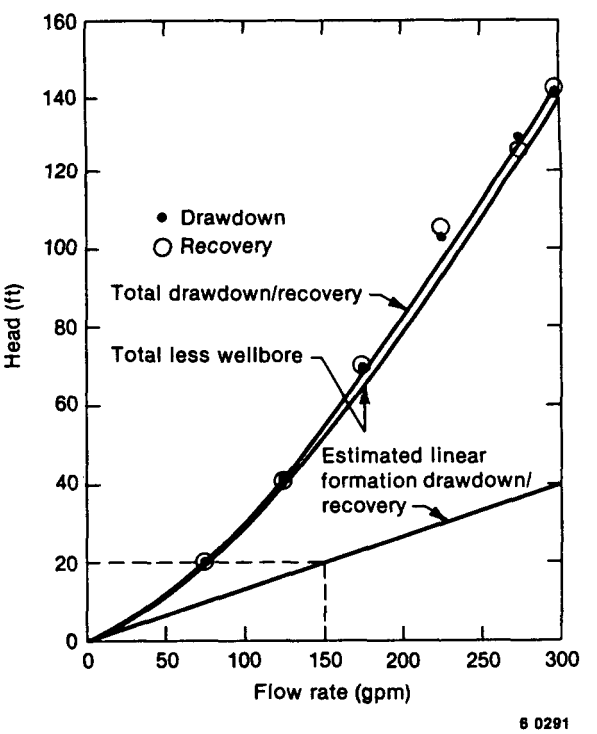

Figure 5. Measured and Linear Drawdown Characteristics

numbers, however, range to considerably higher values because the model may have multiple fracture paths in a given portion of a fracture. Indeed, 120 fracture paths occur in the largest fracture in the system (273 ft radius) and 66 fracture paths occur in the 100 ft radius hydrofracture. Since these tend to be the longest paths in the system, a substantial portion of the flow path may have effective Reynolds numbers greater than one hundred. In the absence of information on fracture roughness, the

analysis was completed by matching values predicted by linear flow relationships to the estimated linear formation drawdown shown in Figure 5.

Figure 6 shows the variation of predicted drawdown head with remote boundary distance and aperture-to-radius ratio for a 150 gpm flow rate. A 100 ft distance was chosen as the best estimate, based partially on the detection, during drilling, of a high transmissivity aquifer at a point near the top of the modeled region. While this does not define the distances to a constant head boundary from the other five faces of the model, the previously discussed 235 second (drawdown) and 130 second (recovery) times tend to confirm the existence of relatively close constant head boundaries. A more precise definition will be provided by work in progress on a fully transient solution. The mean set apertures at the 100 ft remote boundary distance and a 20 ft linear drawdown head are 6.7, 101, and 46 μm for sets 1, 2, and 3, respectively. These values are subject to considerable uncertainty, as to the shape of the spacing and radius distributions, the mean of the radius distribution and the non-linear flow term and may only be accurate to within a factor of three. They may be compared to hydraulic apertures of 6 μm at Stripa (Gale et al., 1985) and 11.8 μm at Chalk River (Raven et al., 1985). In addition to the difference in natural fracture systems, it should be noted that the Raft River fractures may have been opened by the hydraulic stimulation treatment.

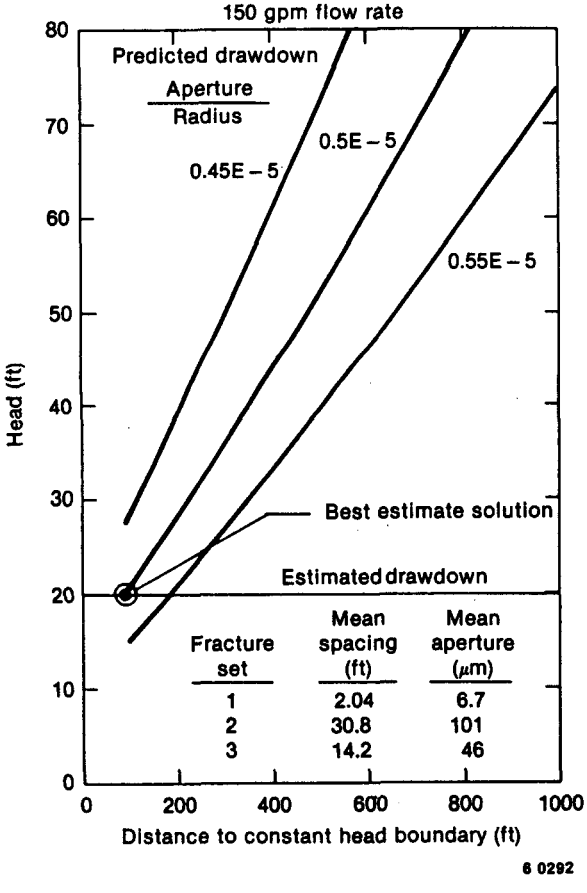

Figure 6. Linear Drawdown Correlation

RECOMMENDED FRACTURE CHARACTERIZATION

A substantial body of work on fracture mapping and characterization has been reported in the interim since this well was completed and tested. Acoustic televiewer data has been complemented by the use of the tube wave device (Paillet and Keys, 1984) which shows the presence of water in a fracture intersecting the wellbore as a discontinuity in an acoustic wave propagated down the borehole. The same authors discuss the use of the heat-pulse flow meter which measures extremely low velocities in the wellbore as a means of detecting fluid bearing fractures. Neutron logging correlated well with conductivity measurements at the Oracle test site in Arizona (Jones et al., 1985) and additional fracture characterization was provided by oriented cores. Doe and Osnes (1985) present methods for determining fracture characteristics from packer testing of individual fractures. The determination of fracture extent, however, may ultimately require other geophysical techniques, such as radar, or the drilling of offset boreholes. Another avenue of approach which may be of benefit in determining fracture extent and fracture distribution in space is the application of existing technology to the description of the structural and hydrothermal processes which created the fracture system. Approaches such as those by Segall and Pollard (1983) and Knapp and Norton (1981) may be developed to correlate borehole characterization data and, in so doing, provide a quantitative description of fracture characteristics not easily obtained from borehole studies.

SUMMARY

A new, dual permeability simulation of fracture system flow has been developed as an effective means of simulating the range of fracture size in a 3D discrete fracture model within the limitations of computer cost and core size. A global model incorporates discrete representations of the larger fractures and a representative element representation of the smaller fractures. The conductivity of the representative element is found by a separate discrete simulation of the smaller fractures. The combined simulation incorporated fractures with radii down to 13.5 to 16 percent of the size of the model. The level of detail and the cost of the simulation are such as to permit, with suitable model extensions, accurate studies of solute transport in fractured geothermal systems.

Definition of the fracture system in this study depended on the form of the distribution of spacing in three-dimensional space and on assumptions as to fracture size distribution. In addition, smaller uncertainties were introduced by the absence of a defined pressure boundary condition and by the presence of non-linear fracture flow. Further information on fracture characteristics will be provided by transient flow simulation and by the addition of a transport model and correlation with measured tracer responses. The uncertainties in these studies can be reduced by more extensive fracture characterization data obtained on the basis of recent advances in packer testing, flow measurement, tube wave and neutron logging and other geophysical methods, and from oriented cores. Further data may ultimately be provided by correlating sampled data with a structural-hydrothermal rationale for the evolution of the fracture system.

This work was funded by the U. S. Department of Energy under Contract No. DE-AC07-76ID01570.

REFERENCES

Clemo, T. M., (1986), Representative Element Modeling of Fracture Systems Based on Stochastic Analysis, Proceedings, Eleventh Workshop on Geothermal Engineering, Stanford University, December 1983, pp 373-379.

Clemo, T. M., (1985), FRACSL Code Development and Correlation of East Mesa Test Results, Proceedings, 10th Workshop on Geothermal Reservoir Engineering, Stanford University, January 1985, pp 287-292.

Dershowitz, W. S., Gordon, B. M. and Kafritsas, J. C., (1985), A New Three-Dimensional Model for Flow in Fractured Rock, Proceedings IAH Symposium on Hydrogeology of Rocks of Low Permeability, Tucson, January 1985, pp 441-448.

Doe, T. W. and Osnes, J. D., (1985), Interpretation of Fracture Geometry from Well Tests, Proceedings, International Symposium on Fundamentals of Rock Joints, Bjorkliden, Sweden, September 15-20, 1985.

Evans, D. D., (1983), Unsaturated Flow and Transport Through Fractured Rock - Related to High-Level Waste Repositories, NUREG/CR-3206, March 1983.

Gale, J. E., Rouleau, A., and Atkinson, L. C., (1985), Hydraulic Properties of Fractures, Proceedings IAH Symposium on Hydrogeology of Rocks of Low Permeability, Tucson, January 1985, pp 1-16.

Huang, C. and Evans, D. D., (1985), A 3-Dimensional Computer Model to Simulate Fluid Flow and Contaminant Transport Through a Rock Fracture System, NUREG/CR-4042, January 1985.

Hull, L. C., (1985), Laboratory Validation of a Dual-Permeability Reservoir Code, Proceedings, Tenth Workshop on Geothermal Reservoir Engineering, Stanford University, January 1985, pp 293-296.

Jones, J. W., Simpson, E. S., Neuman, S. P., and Keys, W. S., (1985), Field and Theoretical Investigations of Fractured Crystalline Rock Near Oracle, Arizona, NUREG/CR-3736, August, 1985.

Knapp, R. B. and Norton, D., (1981), Preliminary Numerical Analysis of Processes Related to Magma Crystallization and Stress Evolution in Cooling Pluton Environments, American Journal of Science, 281, January, 1981, pp. 35-68.

Lamb, H., (1945), Hydrodynamics, Dover Publications, New York.

Mahtab, M. A., Bolstad, D. D., and Kendorski, F. S. (1973), Analysis of the Geometry of Fractures in San Manuel Copper Mine, Arizona, Bureau of Mines RI 7715, January 1973.

Miller, J. D., (1983), A Fundamental Approach to the Simulation of Flow and Dispersion in Fractured Media, Proceedings, 9th Workshop on Geothermal Reservoir Engineering, Stanford University, December 1983, pp 373-379.

Mitchell and Gauthier, Assoc., Inc., (1981), Advanced Continuous Simulation Language (ACSL), User Guide/Reference Manual, Box 685, Concord, Mass. 01742.

Paillet, F. L. and Keys, W. S., Applications of Borehole Geophysics in Characterizing the Hydrology of Fractured Rocks, Proceedings, National Water Well Association Subsurface Investigations Conference, San Antonio, February, 1984.

Priest, S. D. and Hudson, J. A. (1981), Estimation of Discontinuity Spacing and Trace Length Using Scanline Surveys, International Journal of Rock Mechanics and Mining Science and Geomechanics, 18, pp 183-197.

Raven, K. G., Smedley, J. A., Sweezey, R. A. and Novakowski, K. S., (1985), Field Investigations of a Small Groundwater Flow System in Fractured Monzonitic Gneiss, Proceedings IAH Symposium on Hydrogeology of Rocks of Low Permeability, Tucson, January 1985, pp 72-86.

Romm, E. S., (1966), Flow Characteristics of Fractured Rocks, (in Russian). Nedra, Moscow, 283 pp.

Segall, P. and Pollard, D. D., (1983), Joint Formation in Granitic Rock of the Sierra Nevada, Geological Society of America Bulletin, 94, May 1983, pp 563-575.